COLLINS, D. M. (1978). *Acta Cryst.* A**34**, 533–541.
DAVIES, A. R. & ROLLETT, J. S. (1976). *Acta Cryst.* A**32**, 17–23.
DEBAERDEMAEKER, T., TATE, C. & WOOLFSON, M. M. (1985). *Acta Cryst.* A**41**, 286–290.
DEBAERDEMAEKER, T., TATE, C. & WOOLFSON, M. M. (1988). *Acta Cryst.* A**44**, 353–357.
DETITTA, G. T., WEEKS, C. M., THUMAN, P., MILLER, R. & HAUPTMAN, H. A. (1994). *Acta Cryst.* A**50**, 203–210.
GIACOVAZZO, C. (1976). *Acta Cryst.* A**32**, 958–966.
HAUPTMAN, H. (1976). *Acta Cryst.* A**32**, 877–882.
HAUPTMAN, H. (1991). *Crystallographic Computing* 5: *from Chemistry to Biology*, edited by D. MORAS, A. D. PODJARNY & J. C. THIERRY, pp. 324–332. IUCr/Oxford Univ. Press.
HAUPTMAN, H., VELMURUGAN, D. & HAN, F. (1991). *Direct Methods of Solving Crystal Structures*, edited by H. SHENK, pp. 403–406. New York: NATO ASI/Plenum Press.
KARLE, J. & HAUPTMAN, H. (1950). *Acta Cryst.* **3**, 181–187.
KNOSSOW, M., DE RANGO, C., MAUGUEN, Y., SARRAZIN, M. & TSOUCARIS, G. (1977). *Acta Cryst.* A**33**, 119–125.
MAUGUEN, Y. (1979). Thèse, Univ. de Paris VI, France.
MAVRIDIS, I. & PAPAIOANNOU, G. (1995). In preparation.
MILLER, R., DETITTA, G., JONES, R., LANGS, D. A., WEEKS, C. M. & HAUPTMAN, H. A. (1993). *Science*, **295**, 1430–1433.
NARAYAN, R. & NITYANANDA, R. (1982). *Acta Cryst.* A**38**, 122–128.
NAVAZA, A. & NAVAZA, J. (1992). *Acta Cryst.* A**48**, 695–700.
NAVAZA, J. (1985). *Acta Cryst.* A**41**, 232–244.
NAVAZA, J., CASTELLANO, E. E. & TSOUCARIS, G. (1983). *Acta Cryst.* A**39**, 622–631.
RANGO, C. DE, MAUGUEN, Y., TSOUCARIS, G., DODSON, E. J., DODSON, G. G. & TAYLOR, D. J. (1985). *Acta Cryst.* A**41**, 3–17.
RANGO, C. DE, TSOUCARIS, G. & ZELWER, C. (1974). *Acta Cryst.* A**30**, 342–353.
SAYRE, D. (1952). *Acta Cryst.* **5**, 60–65.
SAYRE, D. (1974). *Acta Cryst.* A**30**, 180–184.
TSOUCARIS, G. (1970*a*). *Acta Cryst.* A**26**, 492–499.
TSOUCARIS, G. (1970*b*). *Acta Cryst.* A**26**, 499–501.
WEEKS, C. M., DETITTA, G. T., HAUPTMAN, H. A., THUMAN, P. & MILLER, R. (1994). *Acta Cryst.* A**50**, 210–220.

Acta Cryst. (1995). A**51**, 763–771

The Interpretation of Single-Crystal Diffuse Scattering using Reverse Monte Carlo Modelling

BY V. M. NIELD*

School of Physics and Space Research, University of Birmingham, Edgbaston, Birmingham B15 2TT, England

D. A. KEEN

ISIS Science Division, Rutherford Appleton Laboratory, Chilton, Didcot, Oxfordshire OX11 0QX, England

AND R. L. MCGREEVY

Studsvik Neutron Research Laboratory, S-611 82 Nyköping, Sweden

(*Received* 25 *October* 1994; *accepted* 27 *March* 1995)

Abstract

The scattering from crystals has two components, Bragg and diffuse. In the case of disordered crystalline materials, or those at high temperature, the latter contribution is considerable and contains a great deal of information about any static or thermal disorder in the system. However, interpretation of this diffuse scattering is in general difficult. A new and widely applicable technique for modelling single-crystal diffuse scattering has been developed, which is most useful for the study of disordered crystalline materials. The algorithm, based on the reverse Monte Carlo method, is described in detail, and the information that can be obtained using it is discussed with reference to a study on ice *Ih*.

1. Introduction

The reverse Monte Carlo (RMC) modelling technique, first developed by McGreevy & Pusztai (1988), enables detailed short-range structural information to be obtained from neutron, X-ray and extended X-ray absorption fine structure (EXAFS) measurements (McGreevy & Howe, 1992). A wide variety of different systems has been studied, as diverse as expanded caesium near the critical point (Nield, Howe & McGreevy, 1991) and disordered crystalline solids (Nield, Keen, Hayes & McGreevy, 1992, 1993). The latter group of materials was studied using powder neutron diffraction. There are many recently developed techniques for producing models of crystalline materials, including refinement using simulated annealing in conjunction with both molecular dynamics (Brünger, Kuriyan & Karplus, 1987) and Monte Carlo methods (Newsam, Deem & Freeman,

* Present address: Physics Laboratory, University of Kent, Canterbury, Kent CT2 7NR, England.

1992). Some of these methods refine the model to agree not only with Bragg intensities but also with additional information such as the 'ideal' bond lengths and angles (Wlodawer & Hendrickson, 1982). When applied to powder diffraction data from disordered crystalline materials, the RMC method can be thought of as a refinement technique that models the total scattering, both Bragg and diffuse. The diffuse scattering arises in two ways, from thermal effects – atomic or molecular vibrations, rotations and translations – and from inherent static disorder.

The present paper discusses the extension of the RMC technique to the analysis of neutron single-crystal diffuse scattering (further generalization to include X-ray single-crystal diffuse scattering is trivial). Details of the algorithm are given, together with a comprehensive account of the advantages and limitations of the technique. In this context, the type of information that can be obtained from the RMC method results is considered. Single-crystal data from D_2O ice *Ih* at 20 K, measured on SXD at ISIS (Li *et al.*, 1994), is used to illustrate the technique throughout. A full report on the structure of ice *Ih* is contained in a separate paper (Nield & Whitworth, 1995), which will include a more critical discussion of the results obtained than is appropriate here.

2. The single-crystal reverse Monte Carlo technique (RMCX)

RMC is similar to the Metropolis Monte Carlo technique (Metropolis, Rosenbluth, Rosenbluth, Teller & Teller, 1953) except that one moves atoms to minimize the difference between the measured and calculated structure factors, rather than to minimize the energy of the configuration of particles. No potential function has to be assumed and so the technique is in principle readily applicable to a wide variety of materials. The algorithm is relatively simple, aiding the use of this method and allowing it to be easily modified.

For single-crystal data, the algorithm is based on the definition of the neutron scattering cross section in the static approximation, which gives

$$S(\mathbf{Q}) = (1/N) \sum_{l,k=1}^{N} \langle \overline{b_l} \exp[+i\mathbf{Q} \cdot \mathbf{r}_l(0)] \overline{b_k} \times \exp[-i\mathbf{Q} \cdot \mathbf{r}_k(0)] \rangle, \quad (1)$$

where $\overline{b_l}$, $\overline{b_k}$ are the scattering lengths for atoms l and k, $\mathbf{r}_l(0)$ and $\mathbf{r}_k(0)$ are their positions at $t = 0$ and $\langle \ldots \rangle$ denotes an expectation value averaged over all the initial states of the crystal. N is the number of atoms in the material. Note that the above expression involves an integral over all energies and hence RMCX is used to model total scattering, rather than elastic scattering (Lovesey, 1984, has a more detailed discussion). The expression gives a $t = 0$ instantaneous picture, or 'snapshot', of the whole structure.

To perform any calculations using (1), a configuration of atoms is necessary. In the initial configuration, the atoms are arranged with the correct crystal symmetry, and any information that has been positively determined about their positions in the unit cell is used. Thus, the atoms are normally placed at the time-average sites as obtained from refinement of Bragg intensities. Periodic boundary conditions are applied, requiring an integral number of unit cells in all three directions. (This configuration is known by some authors as a supercell.)

The boundary conditions mean that the configuration is surrounded by images of itself, and the contribution from any atom and its image must be the same. Hence, $S(\mathbf{Q})$ can only be calculated at $\mathbf{Q}$ points which satisfy

$$\mathbf{Q} = 2\pi(h'/an_a, k'/bn_b, l'/cn_c), \quad (2)$$

for lattice parameters a, b, c and a configuration box with n_a, n_b, n_c unit cells in the three directions, h', k', l' are integers. This means that $S(\mathbf{Q})$ can only be calculated on a grid of points in reciprocal-lattice space, with the positions of the points dependent on the number of unit cells. (In terms of the supercell, this expression is readily seen to give the intensity of the Bragg peaks of the supercell.) The coherent part of $S(\mathbf{Q})$, denoted by $F(\mathbf{Q})$, then simplifies to

$$F(\mathbf{Q}) = (1/2\pi N') \left| \sum_i \overline{b_i} \exp(i\mathbf{Q} \cdot \mathbf{R}_i) \right|^2, \quad (3)$$

where the sum is over all N' particles within the configuration box.

The aim of the RMCX is to use (3) to find a configuration of atoms that agrees well with the experimental data. The algorithm is detailed below.

(1) Produce the initial configuration; routinely these contain between 4000 and 40 000 particles, arranged in the known crystal structure as discussed above. The size of the configuration must be compatible with the spacing of the data points [see equation (2)].

(2) Calculate the coherent scattering of the starting configuration using equation (3).

(3) Choose a particle at random and move it a random amount, up to a user-specified maximum, in a random direction. The maximum move size obviously influences how quickly phase space is sampled but also affects the number of moves accepted and therefore the rate of convergence.

(4) The particle–particle distances are checked and if any particles are unphysically close the move is rejected and step 3 is repeated. This prevents any two atoms from being too close to one another. The closest approach values are specified by the user but erroneously large values can easily be noticed if the partial radial distribution functions are calculated once a fit to the data has been achieved. Sharp spikes in the first peaks of

the partial radial distribution functions, sometimes with corresponding troughs elsewhere, indicate that a change in the closest-approach values is required. Additional constraints can readily be incorporated at this stage; for instance, in a molecular system the intramolecular distances can be kept within a specified range.

(5) Equation (3) is used to recalculate the coherent scattering for comparison with the data. In practice, this step is made faster by calculating the contribution due to the moved particle both before and after its move, and taking the difference.

The goodness-of-fit parameter, χ^2, is defined by

$$\chi^2 = \sum_{m=1}^{n_E} [F_E(\mathbf{Q}_m) - F_C(\mathbf{Q}_m)]^2/\sigma_E^2, \qquad (4)$$

where the sum is over all n_E data points at positions $\mathbf{Q}_m$. $F_E(\mathbf{Q}_m)$ is the value of the experimental data for point m and $F_C(\mathbf{Q}_m)$ its calculated counterpart (the incoherent scattering is assumed to have a constant flat level and is subtracted from the experimental data before χ^2 is calculated). The standard deviation σ_E is taken to be independent of $\mathbf{Q}$ and is treated as a parameter of the modelling.

The change in χ^2 resulting from the move is $\Delta\chi^2 = \chi^2_{\text{new}} - \chi^2_{\text{old}}$. If (*a*) $\Delta\chi^2 < 0$ the fit to the data has improved and the move is accepted, (*b*) $\Delta\chi^2 > 0$ the fit to the data has worsened and the move is accepted with probability $\exp(-\Delta\chi^2/2)$.

In the study discussed in this paper, σ_E was taken as 0.01. If extreme values are used, this will obviously affect the calculations significantly. With a very large value of σ_E, the data are ignored (χ^2 is always $\simeq 0$, and so all moves are accepted); with a very small value, the configuration is driven to the local minimum closest to the starting point (there is a negligible probability of moves that make the fit worse being accepted).

(6) The procedure is repeated from step 3 until χ^2 has converged. In practice, for the study on ice it was found that complete convergence took too long and so the fitting was stopped once the rate of convergence was deemed to have become too slow.

As many reciprocal-lattice planes of data as have been measured can be used simultaneously in the fitting procedure. The point group is supplied by the user and the algorithm automatically calculates the scattering over the symmetry-related directions and averages them. In the main study considered here, Bragg scattering was not fitted but, as indicated in the Appendix, preliminary attempts to model Bragg and diffuse scattering together are under way.

2.1. *Information obtainable*

Most methods of obtaining information from crystalline materials analyse only the Bragg scattering. This contains information on the average structure and hence can be used to determine average sites for all the atoms in the material. Anharmonic or anisotropic thermal parameters, or partially occupied 'defect' sites, are used to describe the deviations from the average sites. With the RMCX, a configuration of atoms is obtained that is a representation of the instantaneous structure of the real crystal. From this configuration, it is possible to determine many features of the material under study. In practice, several independent configurations are collected and the results averaged over them all in order to improve statistics.

By using the translation vectors of the unit cell, all of the unit cells of the independent configurations can be superimposed onto one. All local information is lost, but the average atom density can be examined, and properties of the spatial average structure can be obtained. For example, the mean site positions, and mean square displacements in general directions, can be calculated.

Actual atomic separations and the corresponding bond-angle distributions can be calculated directly from the configurations themselves. The values obtained in this case are not necessarily the same as the distances and angles calculated from the mean site positions and comparison can give useful information on local disorder. Diffuse scattering contains information on correlated displacements, and the configuration can readily be probed to explore these. Other useful obtainable information will differ from system to system. For example, in ice the dependence of the displacements of the O atoms on the positions of the neighbouring deuterons was examined. It was also interesting to look at the range of molecular geometries present.

Unless σ_E is chosen to drive the configuration into a local minimum close to the starting point, the RMCX model is one of the most disordered that is consistent with the data. It is therefore likely that any correlations in the model are present in the real material (correlations are not formed by a random increase in disorder), possibly to an even greater degree. However, there may be additional correlations in the real system that are not present in the model, since the data can be fitted without them.

3. Experimental considerations

The scattering in as large a region of reciprocal space as possible should be measured to make the obtained model as realistic as possible (this is discussed in some detail in §6). The main consideration is then the significant time required to make such measurements with good statistics for the inherently weak diffuse scattering. Conventionally, single-crystal neutron disorder diffuse scattering studies have been made at reactor sources, where a monochromatic neutron beam is used, and point-wise surveys of reciprocal space are performed using triple-axis instruments to select elastic scattering. There is, in general, a significant limitation on the highest $\mathbf{Q}$ data accessible. For RMCX purposes, the grid of the

measurement fixes the configuration size except for cases where accurate interpolation of the data is possible.

Time-of-flight (TOF) Laue diffraction as implemented on SXD at ISIS is more flexible and considerably faster. Neutrons of different wavelength (and hence velocity) arrive at the detector at different times. By measurement of the number of arrivals as a function of time, the intensity as a function of wavelength, and hence $|\mathbf{Q}|$, is obtained. SXD has a 64×64 pixel position-sensitive detector, enabling a large volume of reciprocal space to be surveyed for one sample position, even for samples which are not perfectly aligned. Continuous coverage of reciprocal space is achieved and so it is possible to bin the data to allow any reasonable-sized configuration to be chosen as the starting point for the RMCX.

The scattering from either two-axis instruments or time-of-flight Laue diffractometers has to be accurately corrected and normalized. The methods of correction are very similar to those for treating the scattering from liquids and amorphous materials (Howe, McGreevy & Howells, 1989). Corrections are made for background and other non-sample scattering, absorption, multiple scattering and inelasticity. Vanadium scattering is used to normalize for the incident neutron flux profile (in the TOF case) and for the detector efficiency. The corrections for TOF data are the more difficult because most corrections are wavelength dependent. On the other hand, with diffraction data from a monochromatic source of wavelength λ, contamination by neutrons of wavelength λ/n, where n is an integer, is difficult to remove completely and can be a considerable nuisance.

As discussed in the previous section, RMC-generated single-crystal patterns are calculated at discrete points in reciprocal space, determined by the size of the configuration used in the modelling. However, experimentally the data are an average over a region of $\mathbf{Q}$ space determined by the resolution of the instrument and any subsequent binning of the data (TOF case only). This difference between calculation and experiment is not believed to be too serious unless diffuse features that are much sharper than the data bin size are involved. In this case, the value of the binned data is unlikely to be close to the actual data value for the point at which the calculation is performed. A problem of more concern is correction of the data for the breakdown of the static approximation, which is difficult because although a Placzek correction can be applied to take care of the contribution due to the motion of single particles, it does not allow for the scattering from any of the collective modes in the sample, and is itself not accurate for samples of light atoms.

4. Diffuse scattering from ice

Ice *Ih*, the normal form of ice, consists of a regular tetrahedral oxygen network with the H atoms arranged in a disordered manner whilst obeying the Bernal–Fowler rules (Bernal & Fowler, 1933). These state that there is one H atom between neighbouring O atoms and two H atoms near each O atom. The space group is $P6_3/mmc$. This arrangement was used as the starting point for the reverse Monte Carlo calculations discussed in the following section.

The experimental data used in this study were obtained from a sample of deuterated ice *Ih* at 20 K and measured on the SXD diffractometer, as discussed in detail in Li *et al.* (1994). Scattering from the three principal reciprocal-lattice planes was measured in the equatorial plane of the detector. In the eight-molecule orthorhombic cell (see §5), these correspond to:

(1) $(0kl)$, because of the hexagonal symmetry this plane is equivalent to (hhl);

(2) $(h0l)$, because of the hexagonal symmetry this plane is equivalent to $(h,3h,l)$;

(3) a segment of $(hk0)$ corresponding to 30° of the basal plane (which is sufficient in hexagonal symmetry to map out the remainder of that plane).

The data were corrected and normalized and the three planes are shown in Figs. 1–3, respectively. The underlying features, such as the hexagonal rings in the $(h0l)$ and $(hk0)$ planes, are due to disorder of the deuterons subject to the Bernal–Fowler rules. The strongest features that cannot be explained in this way are the streak along $(60l)$, with its associated feature in the basal plane, and the strong scattering at high $\mathbf{Q}$ in the $(0kl)$ plane [see Li *et al.* (1994), for a fuller discussion of the scattering predicted by the Bernal–Fowler rules].

5. Calculations

While the unit cell of ice is hexagonal, it was decided for computational ease to perform the calculations using an

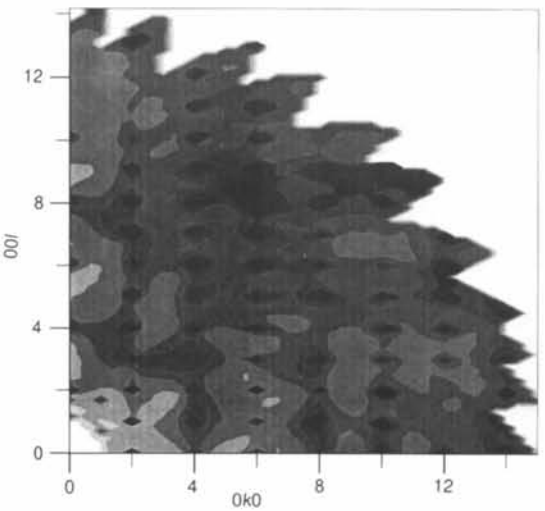

Fig. 1. Experimental neutron scattering pattern in the $(0kl)$ plane from D_2O ice *Ih* at 20 K. Darker shading corresponds to higher contour levels, which are equally spaced between 0.0 and 0.7 and are the same in Figs. 1–5.

eight-molecule orthorhombic cell, with the deuterons initially obeying the Bernal–Fowler rules. $6 \times 6 \times 6$ unit cells were used (1728 molecules). The cell dimensions were taken from the work of Röttger, Endriss, Ihringer, Doyle & Kuhs (1994) to be $a = 4.498$ and $c = 7.323$ Å [and are the same in hexagonal and orthorhombic unit cells, with $b = a$ for the hexagonal cell and $b = 2a\sin(60)$ for the orthorhombic cell]. The oxygen network was initially tetrahedral. The starting positions of the D atoms were varied over a limited range and, within statistics, no differences were found in the final configurations. However, as yet, no comprehensive tests have been performed to discover quite how insensitive the modelling is to the starting point.

For all models, the same closest-approach values were used. These were initially chosen as 2.5, 0.8 and 1.0 Å for O—O, O—D and D—D, respectively, but on examination of the partial radial distribution functions these values were modified to 2.3, 0.5 and 1.0 Å. The small value of the O—D closest-approach distance is consistent with that obtained from a very careful Fourier transform of powder diffraction data (Floriano *et al.*, 1987). σ_E was chosen as 0.01 in all cases. Modelling was stopped when convergence became so slow that several more days of CPU time would have been necessary for minimal changes in the results (all modelling was performed on a digital VAX 4000/60 workstation). In each case, eight independent configurations were obtained. The results from each were in good agreement and so were averaged in order to improve statistics.

By fitting to different numbers of planes and comparing the results obtained in each case it is possible to examine how many data are required to obtain a reasonable answer. Obviously, the more data used in the fitting procedure the more accurate the result is likely to be. The orthorhombic unit cell does not impose the required sixfold symmetry, and so calculating the scattering in planes that should be equivalent to ones used in modelling provides another test of how realistic the model is.

For this reason, three different calculations were performed initially, whereby

(*a*) only the (0*kl*) data were used in the fitting (one-plane fit); this calculation required approximately 12 h CPU time.

(*b*) (0*kl*), (*h*0*l*) and (*hk*0) data were used simultaneously in the fitting (three-plane fit); this calculation required approximately 30 h CPU time.

(*c*) (0*kl*), (*hhl*), (*h*0*l*), (*h*,3*h*,*l*) and (*hk*0) data were used simultaneously (five-plane fit); this calculation required approximately 36 h CPU time.

The long CPU times are a result of the very large number of **Q** and r points; the algorithm has been optimized. A further calculation was performed which, instead of having an equal number of unit cells in each direction, used a configuration of close to equal length (in Å) in all directions (equal size fit). Hence, it had $10 \times 6 \times 6$ unit cells. The nature of the RMCX algorithm, as discussed in §2 and specifically equation (3), indicates that the number of unit cells present alters the required spacing in reciprocal-lattice units (r.l.u.) of the data. Hence, the number of data points for planes containing (*h*00) was larger in this case than previously. For different numbers of cells in the different directions, few reciprocal-lattice points in planes such as (*hhl*) and (*h*,3*h*,*l*) can be modelled, and so only three planes of data were used. The need for equal numbers of unit cells in all directions to fit all possible planes of data is a limitation of the technique that may be significant for some applications.

The importance of measuring and modelling data to high and low **Q** was investigated in two further tests, where data in only a limited region of the (0*kl*) plane were used with RMCX. In the first, no data below $|\mathbf{Q}| = (Q_x^2 + Q_y^2 + Q_z^2)^{1/2} = 8.0$ r.l.u. were used (no low-**Q** fit). In the second, all points above $|\mathbf{Q}| = 11.4$ r.l.u. were ignored (no high-**Q** fit). In both of these limited data range fits, *ca* 1880 data points were used, compared with 2803 in the entire plane. The effect of changing the relative values of the c and a lattice parameters was also investigated.

6. Discussion

The first consideration when modelling data must always be whether there is sufficient data to produce a physically realistic model. As discussed in the previous section, three main calculations were performed, fitting to different numbers of planes of data, but identical in other respects. Fig. 4 shows the fit to the (*h*0*l*) plane from the five-plane fit, and comparison with Fig. 2 shows that it is in excellent agreement with the data. Similarly good fits were obtained in all cases, with agreement in the case of fewer planes of data being slightly better than for the five-plane fit, as would be expected. The slight underlying modulation present in all the fits is a result of the finite configuration size of the model.

Once the fitting was complete, the resultant configurations of atoms were used to predict the scattering for the other planes of data. The one-plane fit gave poor agreement for all other planes and did not pick up any of the strong features that were not a direct consequence of the Bernal–Fowler rules (these rules were built into the starting configuration). For example, neither the streak along (60*l*) in the (*h*0*l*) data [along (39*l*) in (*h*,3*h*,*l*)] nor the strong diffuse scattering at high **Q** in (*hhl*) were reproduced. The scattering calculated in this way for the (*h*0*l*) plane is shown in Fig. 5. The three-plane fit, as might be expected, gave better agreement for the other planes and reproduced the streak along (39*l*) in the (*h*,3*h*,*l*) data but again failed to give the high-**Q** scattering in (*hhl*).

The streak along (60*l*) and (39*l*) is due to correlations in the direction of displacement of neighbouring

molecules. [More details can be found in Nield & Whitworth (1995).] These correlations were not picked up in the one-plane fit, as might be expected if the correlation results in little or no scattering in the (0*kl*) plane. In the three-plane fit, sufficient information about the correlation was present to reproduce the feature due to it in all planes. Hence, the more data used in the modelling, the more likely it is that insight is gained into correlated displacements.

The next area for examination is how well the different models reproduce average features of the data. Mean square displacements along particular directions are given in Table 1. They were calculated by superimposing all unit cells onto one and considering the averaged atom density along a tube centred on the average lattice site

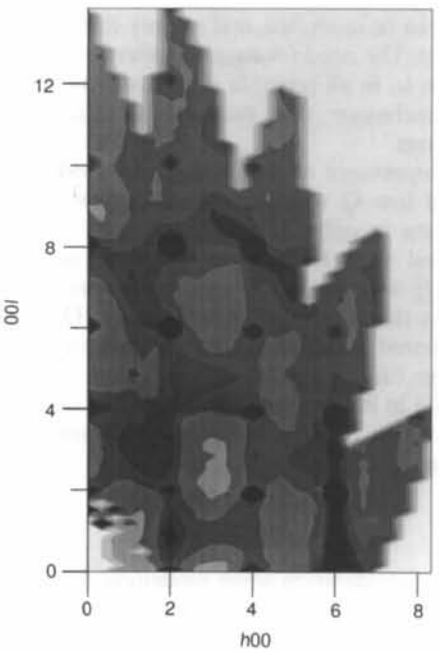

Fig. 2. Experimental neutron scattering pattern in the (*h*0*l*) plane from D_2O ice *Ih* at 20 K.

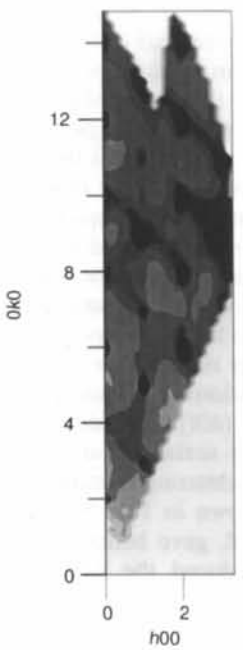

Fig. 3. Experimental neutron scattering pattern in the (*hk*0) plane from D_2O ice *Ih* at 20 K.

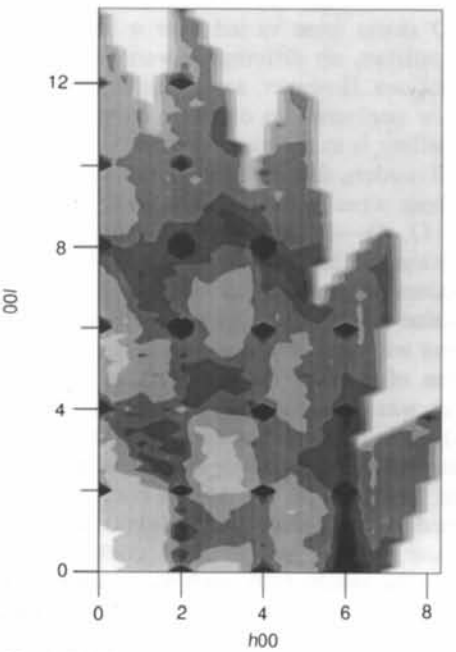

Fig. 4. RMCX five-plane fit to the data of Fig. 2.

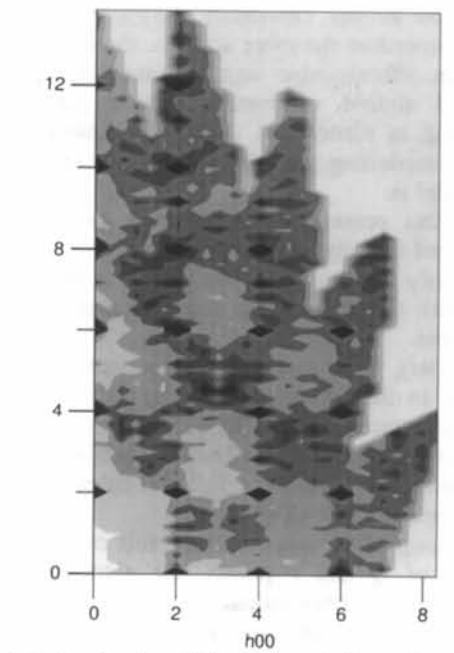

Fig. 5. Scattering in the (*h*0*l*) plane, calculated from RMCX configurations obtained by fitting only to the (0*kl*) plane.

Table 1. *Mean square displacements obtained from the different fits* (Å^2)

$\langle u_j^2 \rangle_{[xyz]}$ gives the mean square displacement in direction [*xyz*] for species *j*, calculated as described in the text. The statistical variation in the last decimal place is given in parentheses.

	Five-plane	Three-plane	One-plane	Equal size	No low **Q**	No high **Q**
$\langle u_O^2 \rangle_{[100]}$	0.0154 (12)	0.0133 (7)	0.0104 (12)	0.0124 (3)	0.0092 (7)	0.0132 (8)
$\langle u_O^2 \rangle_{[010]}$	0.0119 (9)	0.0100 (7)	0.0073 (6)	0.0101 (5)	0.0061 (3)	0.0084 (6)
$\langle u_O^2 \rangle_{[001]}$	0.0132 (5)	0.0109 (7)	0.0080 (8)	0.0112 (8)	0.0065 (4)	0.0086 (7)
$\langle u_D^2 \rangle_{[100]}$	0.0138 (5)	0.0120 (6)	0.0098 (5)	0.0126 (8)	0.0087 (5)	0.0119 (3)
$\langle u_D^2 \rangle_{[010]}$	0.0119 (8)	0.0104 (7)	0.0077 (4)	0.0112 (3)	0.0064 (5)	0.0088 (4)
$\langle u_D^2 \rangle_{[001]}$	0.0132 (7)	0.0107 (5)	0.0082 (4)	0.0107 (6)	0.0067 (2)	0.0084 (3)

and pointing in the required direction. The tube radius was taken as $0.1a$, a compromise between high resolution and good statistics. The values given in Table 1 are averages over all relevant atoms in the eight statistically independent configurations. For comparison, equivalent values obtained for oxygen from Bragg scattering analysis are 0.00862(4) along [001] and 0.00849(3) perpendicular to [001] (Kuhs & Lehmann, 1987). It is immediately apparent that the mean square displacements are greater than those from Bragg analysis and are larger for the fits to larger **Q** ranges of data. If Bragg scattering was fitted at the same time as the diffuse scattering, it would constrain the mean square displacements and so the values would be more realistic. In the present case, no account was taken of experimental resolution and so the static diffuse scattering was broadened, an effect similar to that due to increased thermal vibrations. This, combined with the fact that RMC algorithms tend to maximize with configurational entropy, within the constraints imposed by the data, leads to an increase in the disorder of the atomic arrangements in the configuration, and hence to increased mean square displacements. However, this does not mean that no information on the mean square displacements is obtainable from the RMCX. It can be seen from Table 1 that the trends are the same in all cases, except where insufficient high- or low-**Q** data were used in the modelling.

Accurate mean square displacements in general directions are best obtained from Bragg peak analysis. However, the RMCX model can be used to provide insight into relative values where averaging over all unit cells is not appropriate. For instance, in ice it can give information on the mean square displacement of the oxygen in directions relative to the two deuterons to which it is covalently bonded. It is found, in accord with the work of Kuhs & Lehmann (1986, 1987), that the O atom moves away from its site along the bisector of the molecule in a direction away from the deuterons of the molecule. In an average model, each O atom has four neighbouring D sites, each half-occupied, so this type of information cannot be obtained.

Table 2 shows some mean atomic separations from the various models. These are reasonably consistent and also agree with the results from other sources. The crystallographic work of Kuhs & Lehmann (1986) using the half-hydrogen model with the harmonic approximation

Table 2. *Mean atomic separations* (Å) *and mean bond angles* (°) *for the different fits*

Subscripts *c* and *o* indicate a bond along and oblique to the *c* axis, respectively. O—O is the nearest-neighbour O—O distance, O—D the intramolecular covalent bond length and D—D the intramolecular D—D distance. O—O—O is the mean angle between three neighbouring O atoms and D—O—D the intramolecular angle. The final column gives the distances and angles from the five-plane fit calculated from the mean sites in the unit cell. The figures in parentheses are the statistical variations in the last decimal place.

	Five-plane	Three-plane	One-plane	Equal size	Five-plane (intersite)
$(O—O)_c$	2.743 (6)	2.747 (7)	2.742 (8)	2.745 (5)	2.733 (4)
$(O—O)_o$	2.768 (2)	2.765 (3)	2.764 (2)	2.766 (2)	2.758 (7)
$(O—D)_c$	0.987 (7)	0.990 (7)	0.987 (5)	0.981 (4)	0.970 (3)
$(O—D)_o$	0.999 (2)	0.998 (2)	0.994 (2)	0.997 (3)	0.978 (12)
$(D—D)_c$	1.579 (8)	1.580 (5)	1.576 (5)	1.597 (5)	1.594 (8)
$(D—D)_o$	1.577 (11)	1.579 (4)	1.576 (2)	1.602 (7)	1.593 (19)
O—O—O	109.3 (1)	109.3 (1)	109.3 (1)	109.3 (1)	109.5 (5)
D—O—D	105.8 (3)	105.8 (7)	105.8 (7)	108.3 (12)	109.5 (20)

produced a value of close to 1.0 Å for the O—D intramolecular distance compared with the RMCX mean value of 0.995 Å at 20 K (errors can be read from Table 2). From NMR studies, the D—D intramolecular distance is 1.58(2) Å (Whalley, 1974), which compares very well with the RMCX value of 1.58(1) Å. The D—D distances from the different fits are not entirely consistent, with the value from the equal-size fit in particular being rather high. The reason for this is not yet understood but may relate to the different spacing of the data along some directions in this fit. In particular, it may be related to fine features in the (*h*0*l*) plane. However, the general agreement is very encouraging.

It can be seen in Table 2 that the values of the interatomic spacings along and oblique to the *c* axis are different. However, the ratio of these values depends critically on the c/a ratio. This points to the need to use accurate lattice-parameter values. Some mean bond-angle values are given in Table 2. These are consistent except for the D—O—D angle from the equal-plane fit, this being related to the D—D difference discussed previously. The values obtained in all cases for this intramolecular water angle are in agreement with the value of 107(1)° obtained from Bragg analysis for ice *Ih* (Kuhs & Lehmann, 1987).

The mean sites calculated after superimposing all the unit cells from the five-plane fit (using 20 rather than eight configurations to improve statistics) were used to

determine mean intersite distances and angles, and these are given in the final column of Table 2. Comparison with the second column illustrates the difference between the distances and angles calculated from the average sites and the mean values obtained direct from the configuration. This difference is large in a material such as ice, which has much static disorder. RMCX has the advantage over most techniques of providing both the actual distributions of interatomic separations and bond angles, and the values obtained from the average site positions.

7. Concluding remarks

The newly developed single-crystal reverse Monte Carlo technique (RMCX) is able to produce structural models by fitting solely to neutron single-crystal diffuse scattering. The technique is generally applicable and can be used to provide a large amount of information about the system under study. It is especially useful for investigating the local arrangements in systems with static disorder, where Bragg analysis is only able to determine average structural properties.

In a study on ice *Ih*, in which the D atoms are disordered, it was found that the structure produced by the RMCX agreed well with data from other techniques, although as no Bragg intensities are included at present, mean square displacements are not accurately determined. RMCX allowed a large amount of new information to be obtained from the diffuse scattering, especially concerning the effects of the deuteron disorder. The structure of ice is discussed in detail in Nield & Whitworth (1995). Future developments of the code will include simultaneous modelling of single crystal and powder diffraction data, the modelling of diffuse scattering in non-principal reciprocal-lattice planes and simultaneous modelling of single-crystal Bragg and diffuse scattering, a preliminary account of which is described in the Appendix.

The authors would like to thank M. A. Howe for vast improvements to the RMC codes and the SERC for grants that supported one of us (VMN) and provided the workstation used. Many thanks also go to J.-C. Li, who measured the experimental data used in this study, and to R. W. Whitworth and D. K. Ross for useful discussions.

APPENDIX
Modelling both diffuse and Bragg scattering simultaneously

Ideally, both Bragg and diffuse scattering from single crystals should be analysed simultaneously, as they are in RMC studies of powder diffraction data (Nield, Keen, Hayes & McGreevy, 1992, 1993). This has now been achieved with RMCX in some preliminary work on lead at room temperature. The diffuse scattering was corrected and normalized as indicated in §3. The integrated Bragg intensities were extracted separately from the data and corrections made for extinction, which may be a serious problem because of the size of the crystals normally used in diffuse scattering studies (*ca* 1 cm^3). The Bragg intensities were then normalized by dividing by the sum

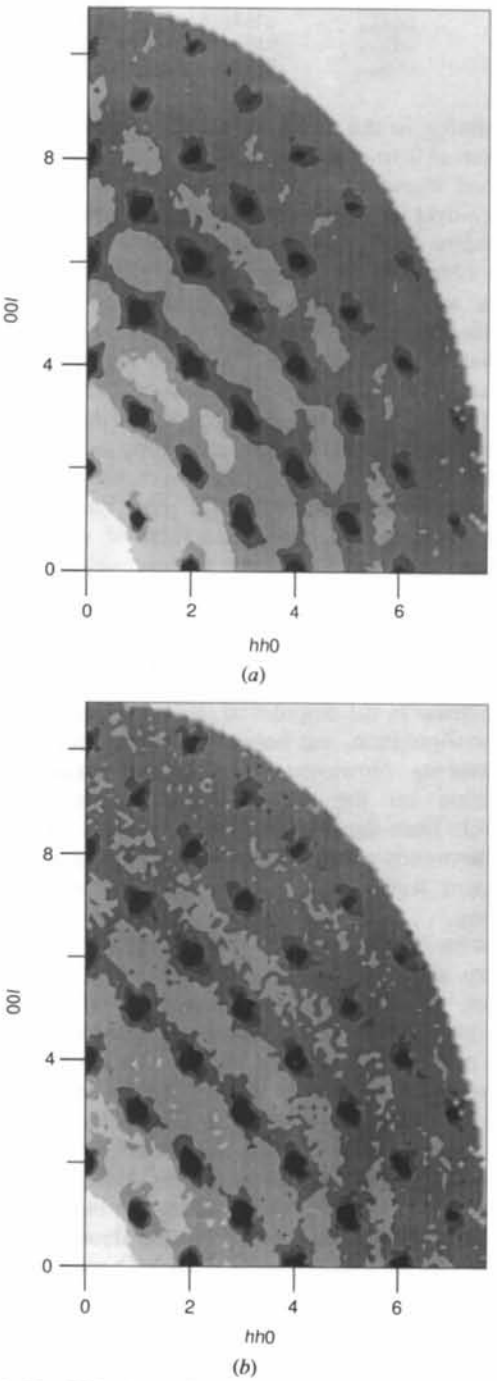

Fig. 6. The (*hhl*) plane of lead at 293 K: (*a*) experimental neutron scattering pattern; (*b*) RMCX fit. The contour levels in these two figures are equally spaced between 0.0 and 2.0, with darker shading corresponding to higher values.

of all such intensities to be used in modelling. Only 37 independent peaks in the same plane as the diffuse scattering were used in this preliminary work. The RMCX algorithm was essentially unchanged, but two goodness-of-fit parameters were calculated, one for Bragg and one for diffuse scattering, and these were then added with a scaling factor β, such that

$$\chi^2_{\text{total}} = \chi^2_{\text{diffuse}} + \beta R_w. \qquad (A1)$$

χ^2_{diffuse} is given by equation (4) of the main text, whilst the weighted R factor, R_w, used for Bragg scattering is defined by

$$R_w = \left\{ \sum_m \left[I_E(\mathbf{Q}_m) - I_C(\mathbf{Q}_m) \right]^2 / \sigma_E(\mathbf{Q}_m)^2 \right\} \times \left[\sum_m I_E(\mathbf{Q}_m)^2 / \sigma_E(\mathbf{Q}_m)^2 \right]^{-1}. \qquad (A2)$$

In this expression, $I_E(\mathbf{Q}_m)$ is the normalized experimental integrated intensity of the mth Bragg peak and $I_C(\mathbf{Q}_m)$ its calculated counterpart. $\sigma_E(\mathbf{Q}_m)$ is the corresponding experimental error. To fit both types of data well it was necessary initially to make the scaling factor β very large, so that a very good fit to the Bragg scattering was obtained (R_w of the order 10^{-4}). β was then decreased in stages, with convergence achieved at each stage. It is hence a very computationally expensive procedure.

Fig. 6 shows the experimental diffuse scattering from SXD for lead at 293 K, together with the RMCX fit. The agreement is good considering the poor statistics and large systematic errors in the data. (The systematic errors arose largely because the measurement was made with a small position-sensitive detector and the exact sample angle for each detector position is not known so that the joining of different segments of data could not be done with sufficient accuracy.) Good agreement was also obtained with the Bragg intensities, with a weighted R factor of 0.05, close to the 0.03 obtained by refinement of the Bragg peaks alone. The mean square displacements in the two cases were also in reasonable agreement, with a value of 0.029 (3) Å^2 in the present study and 0.024 (1) Å^2 from analysis solely of the Bragg intensities. This gives encouragement that Bragg and diffuse scattering can be fitted simultaneously. Work on optimizing the algorithm is continuing.

References

BERNAL, J. D. & FOWLER, R. H. (1993). *J. Chem. Phys.* **1**, 515–519.
BRÜNGER, A. T., KURIYAN, J. & KARPLUS, M. (1987). *Science*, **235**, 458–460.
FLORIANO, M. A., KLUG, D. D., WHALLEY, E., SVENSSON, E. C., SEARS, V. F. & HALLMAN, E. D. (1987). *Nature (London)*, **329**, 821–823.
HOWE, M. A., MCGREEVY, R. L. & HOWELLS, W. S. (1989). *J. Phys. Condens. Matter*, **1**, 3433–3451.
KUHS, W. F. & LEHMANN, M. S. (1986). *Water Sci. Rev.* **2**, 1–65.
KUHS, W. F. & LEHMANN, M. S. (1987). *J. Phys.* **48**(C1), 3–8.
LI, J. C., NIELD, V. M., ROSS, D. K., WHITWORTH, R. W., WILSON, C. C. & KEEN, D. A (1994). *Philos. Mag.* B**69**, 1173–1181.
LOVESEY, S. W. (1984). *Theory of Neutron Scattering from Condensed Matter*, Vol. I. pp. 29–30. Oxford Univ. Press.
MCGREEVY, R. L. & HOWE, M. A. (1992). *Ann. Rev. Mater. Sci.* **22**, 217–242.
MCGREEVY, R. L. & PUSZTAI, L. (1988). *Mol. Simul.* **1**, 359–367.
METROPOLIS, N., ROSENBLUTH, A. W., ROSENBLUTH, M. N., TELLER, A. H. & TELLER, E. J. (1953). *J. Chem. Phys.* **21**, 1087–1094.
NEWSAM, J. M., DEEM, M. W. & FREEMAN, C. M. (1992). *Natl Inst. Stand. Technol. Spec. Publ.* No. 846, pp. 80–91.
NIELD, V. M., HOWE, M. A. & MCGREEVY, R. L. (1991). *J. Phys. Condens. Matter*, **3**, 7519–7525.
NIELD, V M., KEEN, D. A., HAYES, W. & MCGREEVY, R. L. (1992). *J. Phys. Condens. Matter*, **4**, 6703–6714.
NIELD, V. M., KEEN, D. A., HAYES, W. & MCGREEVY, R. L. (1993). *Solid State Ion.* **66**, 247–258.
NIELD, V. M. & WHITWORTH, R. W. (1995). *J. Phys. Condens. Matter.* Submitted.
RÖTTGER, K., ENDRISS, A., IHRINGER, J., DOYLE, S. & KUHS, W. F. (1994). *Acta Cryst.* B**50**, 644–648.
WHALLEY, E. (1974). *Mol. Phys.* **28**, 1105–1108.
WLODAWER, A. & HENDRICKSON, W. A. (1982). *Acta Cryst.* A**38**, 239–247.

Acta Cryst. (1995). A**51**, 771–790

Diffraction by Disordered Polycrystalline Fibers

BY W. J. STROUD AND R. P. MILLANE*

Whistler Center for Carbohydrate Research, Purdue University, West Lafayette, Indiana 47907-1160, *USA*

(*Received* 9 *September* 1994; *accepted* 15 *February* 1995)

Abstract

X-ray diffraction patterns from some polycrystalline fibers show that the constituent microcrystallites are disordered. The relationship between the crystal structure and the diffracted intensities is then quite complicated and depends on the precise kind and degree of disorder present. The effects of disorder on diffracted intensities must be included in structure determinations using diffraction data from such specimens. Theory and algorithms are developed here that allow the full

* To whom all correspondence should be addressed.